JACS
JOURNAL OF THE AMERICAN CHEMICAL SOCIETY
Article
pubs.acs.org/JACS

Reaction of Phthalocyanines with Graphene on Ir(111)

Simon J. Altenburg,[†] Marie Lattelais,[‡] Bin Wang,[∥] Marie-Laure Bocquet,[‡,§] and Richard Berndt*[,†]

[†]Institut für Experimentelle und Angewandte Physik, Christian-Albrechts-Universität zu Kiel, D-24098 Kiel, Germany
[‡]Laboratoire de Chimie, Ecole Normale Supérieure de Lyon, CNRS, Université de Lyon, F69007 Lyon, France
[∥]School of Chemical, Biological, and Materials Engineering, University of Oklahoma, 100 E. Boyd St., Norman, Oklahoma 73019-1004, United States

Supporting Information

ABSTRACT: Iron phthalocyanine (FePc) is adsorbed to graphene on Ir(111) at cryogenic temperature. In addition to mobile FePc with four lobes, imaging and spectroscopy with a scanning tunneling microscope reveal immobile molecules that exhibit fewer lobes. A reversible transformation between four- and three-lobed molecules has been induced by current injection. The data are consistent with chemical bonding of lobes to graphene on Ir, pinning down the graphene area toward Ir. Similar observations are made from NiPc, CoPc, CuPc, and H_2Pc. The experimental findings can be explained by ab initio calculations, which suggest that a Diels–Alder-type reaction may be involved with an allyl unit of graphene in the top-fcc moiré registry.

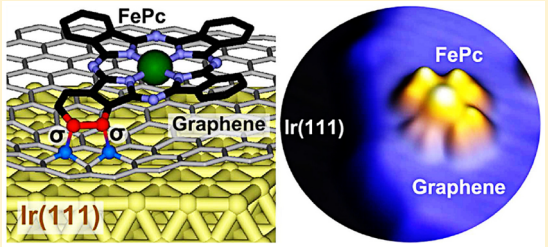

INTRODUCTION

With its exceptional charge mobility, graphene holds promise for applications in electronics and nanosensors.[1] To tailor its properties, chemical functionalization using various molecules[2−12] including phthalocyanines[13−18] is being actively pursued. On single crystal surfaces, graphene layers may be grown with a high degree of perfection. The substrates interact with the graphene layer and modify its electronic properties.[19−26] Superstructures that involve periodic modulations of geometric and electronic properties are observed on most transition metals. These local variations of adsorbed graphene layers offer additional opportunities to achieve chemical functionalization.

The Diels–Alder (DA) reaction, activated by heat or light, is a prototypical cycloaddition[27,28] between butadiene (diene) and ethylene (dienophile) to form a six-membered ring cyclohexene. It involves six π electrons and fulfills the Woodward-Hoffman selection rules for an orbital symmetry-allowed process.[29,30] This classical pericyclic reaction has recently been demonstrated on graphene wafers, with graphene mostly reacting as an ethylene fragment.[31−33] To date, however, concerted cycloadditions have not been observed on metal–supported graphene.

Here we report on the interaction of iron-, cobalt-, nickel-, copper-, and H_2-phthalocyanines (FePc, CoPc, NiPc, CuPc, H_2Pc) with graphene on Ir(111) at cryogenic temperature. Scanning tunneling microscopy (STM) and spectroscopy show that deposition of low coverages of these molecules leads to distinct adsorbed states. In addition to a weakly bound state observed previously,[13,34] the Pc molecules may bind to the graphene overlayer with one to three Pc lobes. The experimental findings are discussed on the basis of ab initio calculations. The calculations reproduce important aspects of the experimental data and show that a nonclassic cycloaddition occurs between a C2 part of FePc and a C3 part of graphene. This new reaction is likely to occur with related molecules, e.g., metal porphyrins, as well.[35]

Depending on the strength of the interaction with a metal substrate, graphene layers may be categorized as physisorbed (weakly interacting) or chemisorbed. Graphene on Ir(111) is an intriguing case.[36−39] On one hand, its electronic states around the Fermi level closely resemble those of pristine graphene. On the other hand, a weak covalent interaction resulting from π-d hybridization occurs in those areas of the moiré pattern where C atoms are located atop Ir atoms. This peculiar interaction suggests the presence of unsaturated dangling bonds that are located on C atoms in hollow sites of the Ir lattice. Some important properties of graphene on Ir(111) are summarized in Figure 1.

METHODS

Experiment. Experiments were performed with a home-built scanning tunneling microscope operated at 5.2 K at a base pressure below 10^{-8} Pa. Ir(111) surfaces were cleaned by cycles of Ar ion bombardment and annealing. Graphene films were grown by exposing the sample to $\approx 6 \times 10^4$ Pa·s of C_2H_4 at room temperature and subsequent annealing at ≈1400 K. This procedure leads to a partial coverage of Ir(111) by highly ordered graphene.[40] Au and Ni tips were electrochemically etched. Both kinds of tips were further treated in situ by heating and Ar ion bombardment. Phthalocyanines were sublimated from a home-built Knudsen cell onto the sample held at a temperature below 12 K. Commercial phthalocyanines (purities FePc: 90%, NiPc:

Received: May 29, 2015
Published: July 6, 2015

DOI: 10.1021/jacs.5b05558
J. Am. Chem. Soc. 2015, 137, 9452−9458

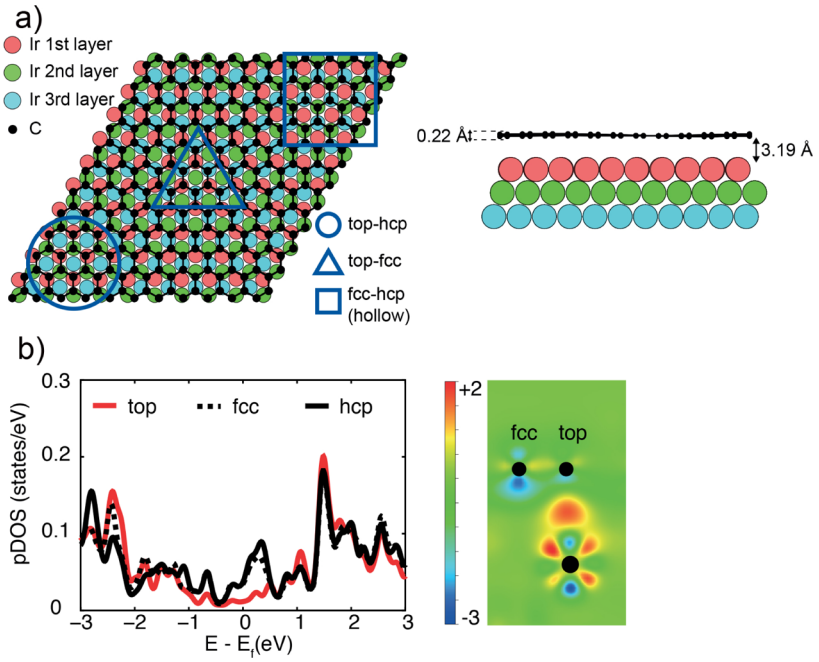

Figure 1. (a) DFT + D2 optimized structure of graphene on the Ir(111) surface. A supercell of (10 × 10) carbon atoms on a (9 × 9) patch of Ir (111) was used. Top view: Three symmetric registries of C pairs of the graphene layer on Ir are highlighted. Side view: The graphene layer is almost flat (0.2 Å height variation) and lies at a distance of ∼3.2 Å above Ir. (b) π-d hybridization between graphene and Ir. Left: The pDOS on representative carbon atoms of graphene on Ir(111). Top C and hollow (fcc and hcp) C of graphene exhibit distinct resonances near the Fermi level. Right: Side view of calculated charge transfer upon adsorption at a top-hollow region of graphene on Ir showing the presence of an out-of-plane p state (dangling bond) on hollow C atoms. Blue (red) color corresponds to loss (gain) of electron density (in e·nm^{-3}).

85%, H_2Pc: 98%, CoPc: 97%, CuPc: 97%) were cleaned in ultrahigh vacuum by heating the Knudsen cell over a period exceeding 12 h to a temperature below the detected onset of sublimation. Spectra of dI/dV were acquired by a standard lock-in technique using a sinusoidal modulation at a frequency of 10 kHz and an amplitude of 15 mV$_{rms}$.

Theory. Periodic density functional theory (DFT) calculations of the entire interface were performed using the VASP code.[41−43] The Ir(111) slab comprised three Ir layers embedded in 16 Å of vacuum space, ensuring almost 10 Å between FePc and the bottom slab of the adjacent supercell. The pristine FePc molecule has a spin S = 1 (2 unpaired electrons) localized on the Fe center, which almost survives upon peripheric covalent bonding of the macrocycle on the graphenic surface. Hence we conducted spin-polarized calculations within the GGA-PBE framework[44,45] followed by a semiempirical Grimme dispersion correction (DFT-D2)[46] as available in the latest version of VASP.[47] Structures are optimized at the Γ point of the surface Brillouin zone, while energies result from a static calculation on a more dense k-grid (i.e., 3 × 3 × 1). Concerning spectroscopic measurements, it is known that the PBE functional consistently reproduces the HOMO of a phthalocyanine molecule but not the HOMO−LUMO gap,[48] whereas hybrid functionals like PBE0[49] provide a more accurate HOMO−LUMO gap. Since hybrid functionals are much more time demanding than PBE, the whole interfacial system was not tractable with PBE0. We thus computed the PBE0 DOS of the system without the Ir(111) at the geometry optimized with PBE+D2.

RESULTS

Experiment. On metal surfaces, FePc displays a typical cloverleaf shape with four lobes[50−55] when imaged with low-temperature STM after deposition at low temperature. On epitaxial graphene, we find that isolated four-lobe molecules are very mobile under the influence of the STM tip and tend to form dimers (Figure 2a) or larger clusters during scanning. Within clusters, these molecules can be resolved and exhibit four lobes. We interpret them as being physisorbed as on graphite.[56] Like on other decoupling substrates,[57,58] each lobe appears split in occupied state images, featuring a major contribution of the nodal a_{1u} orbital.

Some molecules are found in an immobile, bound state with only three protruding lobes (three-lobe species, Figure 2a). Missing lobes (marked by white dots in Figure 2c) are always situated in the same area of the moiré pattern—at the right half of the moiré rhombus—where the C atoms of the two sublattices are located on top and hcp or fcc hollow adsorption sites of the underlying Ir surface.[59] The fcc hollow C atoms in this moiré area present a localized dangling bond, i.e., an out-of-plane electron-deficient state (Figure 1b). From atomically resolved STM topographs we verified that the graphene and moiré lattices had the same orientation. In three-lobe FePc, the axis defined by the two lobes next to the missing one was rotated by ≈15° from the closest moiré lattice direction.

A vast majority of the FePc molecules on graphene were in the three- or four-lobe states. Occasionally, we observed molecules lacking two (two-lobe species, Figure 2a) or more lobes (cf. Figure 5). Like the three-lobe species, they were immobile, and spectroscopy of their electronic states was feasible.

Manipulation experiments were performed on the majority species, three- and four-lobe molecules. We repeatedly observed that these two species could be converted into each other. Figure 3 shows an example of switching in a dimer of four-lobe FePcs to the three-lobe state and back. Switching from four to three lobes occurred when electrons were injected into the unoccupied orbitals, usually at sample voltages V > 1.5 V. It could only be induced on those molecules that exhibited a specific registry with the graphene and moiré lattices, to allow for bond formation to graphene as discussed below. Three-lobe molecules could be switched to the four-lobe state by electron removal from the highest occupied molecular orbital (HOMO)

DOI: 10.1021/jacs.5b05558
J. Am. Chem. Soc. 2015, 137, 9452−9458

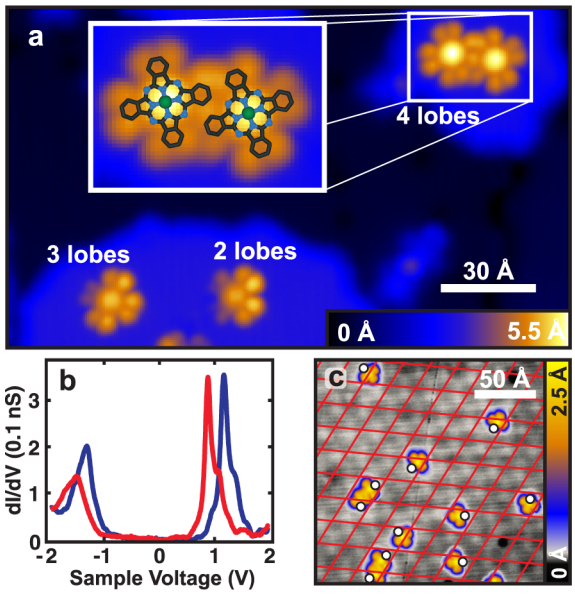

Figure 2. (a) STM topograph of FePc on graphene islands on Ir(111) (sample voltage $V = -1.3$ V, tunneling current $I = 100$ pA); black: Ir substrate, blue: graphene layer, orange, and yellow: FePc in different states (four, three and two-lobe species). Inset: Zoom-in view of the four-lobe FePc dimer overlaid with the molecular structure. (b) dI/dV spectra obtained at the center of the four-lobe (blue) and three-lobe (red) species. (c) Large-scale topograph ($V = -1$ V, $I = 100$ pA) of three-lobe FePc molecules on graphene on Ir(111) with superimposed red lines showing the moiré lattice. The positions of the missing lobes of the molecules are indicated by white dots. The three-lobe molecules exhibit different orientations, but the white dots are exclusively located in the same right upper half of the moiré unit cell, corresponding to one top-hollow region in the moiré pattern. Additionally, the axis defined by the two lobes next to the missing one is always rotated by ≈15° from the closest moiré lattice direction. Two dimers of three-lobe FePc are discernible. They occupy two adjacent moiré cells resulting in one missing lobe per unit cell.

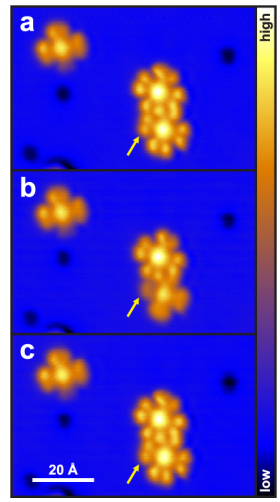

Figure 3. Sequence of constant-current images ($V = -1.2$ V, $I = 100$ pA) showing reversible switching between four- and three-lobe states. The molecular lobe involved in the process is marked by a yellow arrow. (a) Before manipulation. The FePc molecules on the right-hand side are in the four-lobe state. (b) After applying a voltage ramp from 1 to 3 V at the center of the lowest FePc molecule, this molecule is transformed to the three-lobe state. A sudden jump of the current had occurred at a sample voltage of 1.25 V indicating the switching event. (c) After applying a voltage ramp from −1 to −3 V at the center of the same molecules, the molecule has returned to the four-lobe state. The switching event had been signaled by an abrupt change of the current at $V = -1.1$ V.

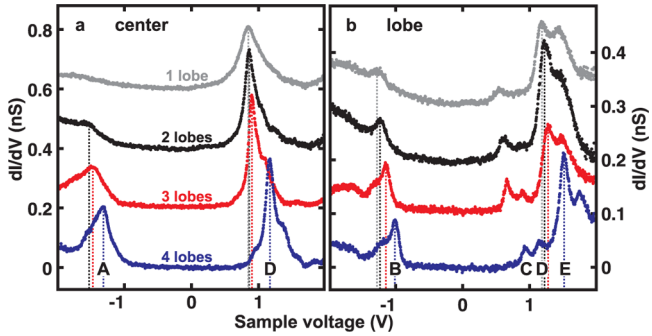

Figure 4. (a) Spectra of the differential conductance obtained at the center of FePc showing four (blue), three (red), two (black), and one lobe (gray), respectively. (b) Spectra obtained at visible lobes. Prominent peaks are indicated by dotted lines and labeled A to E. All peaks shift to lower voltages with decreasing number of visible lobes.

at $V < -1.1$ V with sufficiently high currents ($I > 100$ pA). It should be noted that the attempts to manipulate a molecule often led to less favorable results. For example, transfer of a molecule from the sample to the tip frequently occurred. Owing to the mobility of four-lobe molecules, obtaining clear observations of switching from three lobes to four lobes was difficult. However, it was achieved in cases where the mobile product was trapped by neighboring molecules.

Figure 2b displays conductance spectra (dI/dV) of four- and three-lobe molecule centers. Two peaks corresponding to molecular orbitals can be observed in both cases, the main difference being a downward shift of the peaks by 200−300 mV in the three-lobe state. Additional states are resolved at the molecular lobes (Figure 4). Spectra of two- and one-lobe species show a further downward shift of the peaks (Figure 4). The dI/dV maps indicating the spatial distribution of the states are shown in Figure 5.

The binding of one or more lobes to graphene is not unique for FePc. Additional experiments were performed with H_2Pc, CoPc, CuPc, and NiPc (Figure 6). The experimental results are closely related to the observations from FePc. All molecules are found in both three- and four-lobe states. Obviously, the capability of assuming a three-lobe state is not linked to the central ion.

For Pcs on metal surfaces, the loss of two H atoms from the outer macrocycle leads to a disappearance of a lobe.[60,61] Here we discard this scenario because the threshold voltage required for switching is well below that needed for H removal (>3−3.5 V).[60,62] Second, the reversibility of the switching in our experiments is inconsistent with irreversible C−H scissions.

A possible reason for the three-lobe appearance of FePc molecules could be the presence of defects in the graphene layer. To explore this possibility, manipulation experiments were performed to laterally move three-lobe molecules and inspect the area underneath. We repeatedly found intact graphene at the original position of the missing lobe of the three-lobe molecule. An example is shown in Figure 7. These observations demonstrate the three-lobe state of the molecules is not caused by defects. It should be noted that sometimes defects were found at the original positions. However, it is unclear whether these defects were present before the

DOI: 10.1021/jacs.5b05558
J. Am. Chem. Soc. 2015, 137, 9452−9458

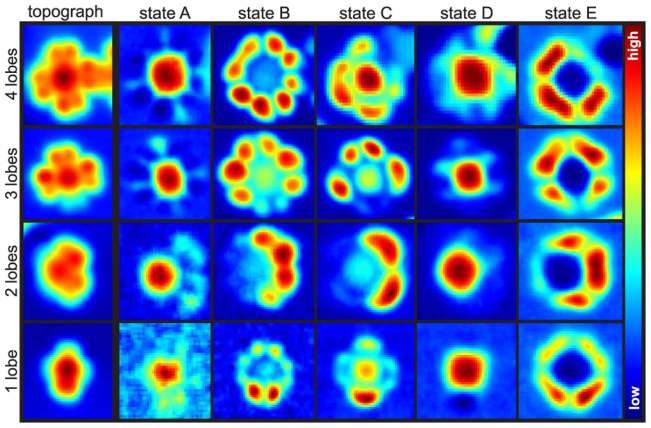

Figure 5. Topographs (left column) and constant current dI/dV maps of FePc with four lobes to one lobe (rows). The dI/dV maps were obtained at the energies of the specified states (A to E in Figure 4). States A and D are located at the center, states B and C at the visible lobes, and state E is located between the visible lobes. Note that for the four-lobe molecule (top row) a neighboring molecule moved closer in the maps of states C, D, and E, suppressing some features in the dI/dV maps. However, comparing the symmetry of the states to those of the other species, the symmetry of the visible four-lobe features is preserved. State C of the three-lobe species shows an additional node on the middle lobe that is not observed from any other species.

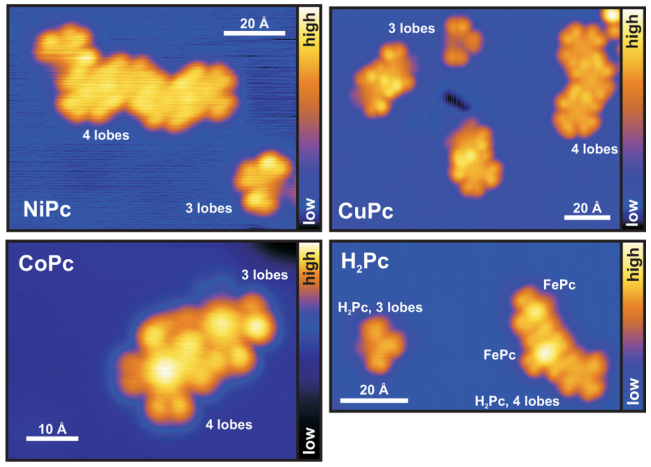

Figure 6. Constant current images (I = 100 pA) of diverse phthalocyanines on graphene on Ir(111). The images of CuPc (V = −2.0 V), CoPc (V = −2.5 V), and NiPc (V = −2.5 V) show the respective molecules in their three- and four-lobe states. H_2Pc (V = −1.0 V) was codeposited with FePc. The molecules are discernible by the apparent heights of the molecular centers. While FePc exhibits a protrusion, the center of H_2Pc appears low. Three- and four-lobe states of H_2Pc are observed.

manipulation was carried out. In any event, they are not required to obtain a three-lobe state of FePc.

Theory. We used DFT calculations to investigate a type of reaction with graphene that preserves the Pc molecule, namely the Diels–Alder cycloaddition. Graphene classically reacts via even units, C2 or C4. However, graphene on Ir exhibits dangling bonds at C atoms of the (top, hollow) region (Figure 1b). Therefore, an allyl C3 unit of graphene has also been considered in our calculations (Figure 9a). Concerning Pc, we found three interacting fragments that react with 2 or 4 electrons (Figure 8).

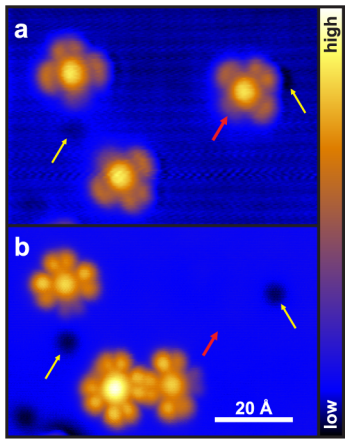

Figure 7. (a) Constant current image (V = 2 V, I = 100 pA) of three FePc molecules in a three-lobe state. Two defects in the graphene sheet appear as depressions (marked by yellow arrows). The position of the binding lobe of one of the FePcs is indicated by a red arrow. (b) Image (V = −1.2 V, I = 100 pA) of the same area recorded after a series of tip-induced manipulations. The upper left FePc and the defects are unchanged. The different appearances of the FePC molecules in (a) and (b) are caused by the different sample voltages used. The molecules originally located at the upper right corner have been moved laterally revealing the area underneath. No defect is discernible at its original binding site (red arrow).

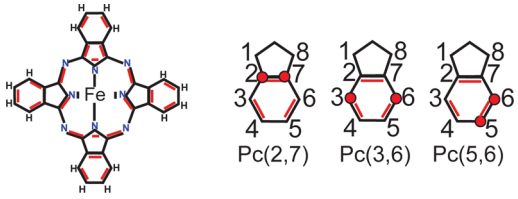

Figure 8. Investigated positions of the newly formed σ bonds on the binding lobe of FePc. Left: FePc resonance structure with double bonds marked in red. Right: Three grafting positions on one Pc lobe that lead to cycloaddition with graphene. Pc(2,7), Pc(3,6), and Pc(5,6) involve 2, 4, and 2 π electrons, respectively.

An exhaustive screening of possible cycloadditions (see mechanisms and models in Figure 9b and energies in Table S1 of the Supporting Information) lead to the most favorable cycloadduct shown in Figure 9a, where a C2 unit of the isoindole moiety binds covalently to a C3 unit of epitaxial graphene in a top-fcc registry. Unpaired electrons left on grafted graphene will further enhance the bonding of graphene to the Ir substrate and the quenching of radicals. This induced covalent bonding of graphene to Ir stabilizes the product C3-Pc(5,6) with respect to pristine physisorbed FePc. As a result, the energy of C3-Pc(5,6) is only moderately increased by 0.4 eV compared to the physisorbed state (see Supporting Information, Table S1). Moreover, this species displays a misorientation of ≈15° with respect to the moiré pattern as observed in the experiments. Finally, the characteristic "missing-lobe" contrast is reproduced in STM image simulations (inset of Figure 10a). The sideview in Figure 10a shows that the buckling of graphene below the bonded lobe is significant in magnitude but limited to a few atoms (6–7 out of 200) similar to the case of an Ir tetramer.[63] We hence expect that such deformation will occur with other strong adsorbates on graphene on Ir.

DOI: 10.1021/jacs.5b05558
J. Am. Chem. Soc. 2015, 137, 9452–9458

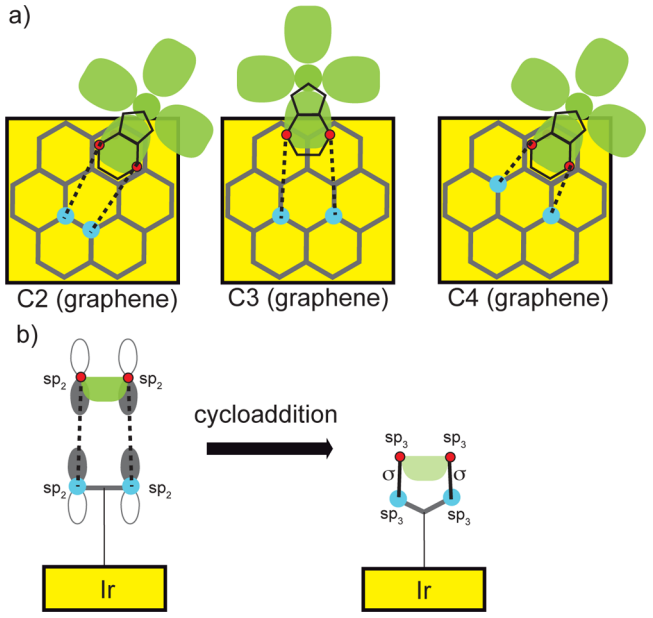

Figure 9. Principle of a cycloaddition between FePc and epitaxial graphene on Ir. (a) Top views indicate the registries of the C2, C3 and C4 graphene fragments on Ir and the Pc(3,6) fragment of FePc for example. Active C atoms forming new σ bonds from FePc (graphene) are red (blue) spheres. Prior to cyclization, the graphene–Ir interaction can be ascribed to a physisorption with chemical modulation. (b) Side views show the approach of the two partners in parallel planes enabling π orbital overlap and eventually forming a cycloadduct with two new σ bonds. The reacting molecular lobe is pinned down toward the Ir substrate, which results in its lower apparent height in STM images. Simultaneously, new bonds to Ir pin the graphene area to the substrate.

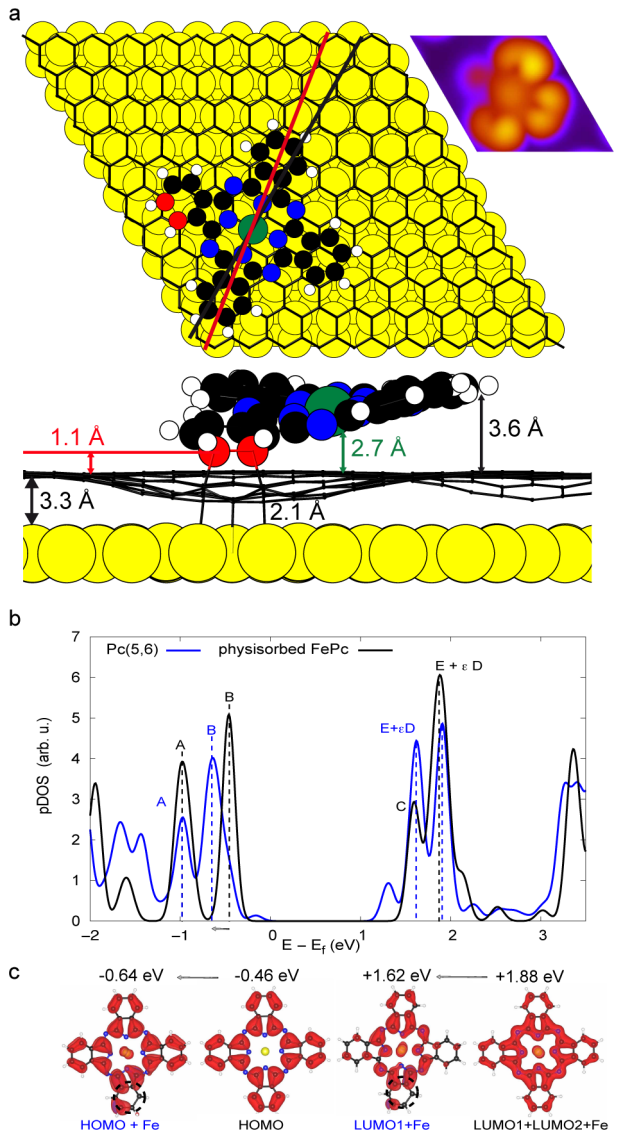

Figure 10. (a) Structure of the proposed cycloadduct C3-Pc(5,6) optimized with spin-polarized DFT+D2. A unit cell of the periodic calculation, which corresponds to the moiré cell, is depicted. The inset shows a simulated constant-current STM image of the moiré cell at −1.2 V. The adduct lobes display a small misalignment of 13–14° with respect to the moiré direction (black line). (b) Projected DOS onto out-of-plane atomic states of physisorbed FePc (black) and the C3-Pc(5,6) adduct (blue) on Ir-free graphene calculated at the PBE0 level. (c) Partial charge densities displayed for a 0.1 eV energy range around the energies of peaks A–D. Isosurfaces are shown for 5×10^{-1} e·nm^{-3} at negative energies and for e·nm^{-3} at positive energies. The isosurfaces resemble mixtures of the indicated orbitals. For the C3-Pc(5,6) adduct the LUMO levels are no longer degenerate.

Other fragments of Pc bonded to C3 graphene lead to more endothermic products (see Supporting Information, Figure S2 and Table S1). In addition, the lobes of these products are perfectly aligned with the moiré pattern, in contrast to the experimental result, and they are discarded. Two other registries of graphene, top-hcp and fcc-hcp, have also been investigated as grafting positions and turned out to be less reactive or unreactive, respectively. These findings match the observed unique position of the three-lobe species in the moiré cell. On the Ir surface, the classic even units of graphene, C2 and C4, yield cycloadducts which are significantly less stable (1.8–2.4 eV for the same reactive region on graphene, see Supporting Information, Table S1). Finally, in the calculation, removal of the Ir support destroys the C3-Pc(5,6) product, which evolves back to a physisorbed FePc. Ir patently plays a critical role in the proposed chemical reaction. The electronic activation is consistent with the following orbital frontier scenario: the LUMO of the FePc gains one electron upon electronic injection that will strongly interact with the singly occupied C3 state of graphene.

In order to theoretically analyze the spectroscopic data of Figures 2b and 4, we replaced the PBE-GGA functional by a hybrid PBE0 functional that can better account for exchange.[49] The projected density-of-states (pDOS) at the PBE0 level (Figure 10b) was obtained neglecting the Ir substrate with the Pc molecule frozen in the previously calculated PBE-GGA geometry of the C3-Pc(5,6) state. The calculated HOMO–LUMO gap (2.2–2.5 eV) is similar to the STS result. Partial charge density maps resolved in energy (Figure 10c) are used to interpret peaks in the pDOS and the corresponding dI/dV spectra and maps. The experimental peaks A, B, C, and E are found in the pDOS. State D cannot unambiguously be identified, presumably because it is masked by states C or E. Importantly, the downshift of states B and E of C3-Pc(5,6) compared to pristine FePc by 200–250 meV matches the experimental results.

Finally it should be mentioned that previous studies of FePc on graphene on Ir focused on molecular self-assembly at high coverages and did not report the new effects presented here.[13,34] Indeed, the reactivity of FePc unveiled here is specific

DOI: 10.1021/jacs.5b05558
J. Am. Chem. Soc. 2015, 137, 9452–9458

to isolated molecules. At high coverages, we compute that FePc molecules gain 0.3 eV per molecule by forming a periodic network, which removes the driving force for the reaction with graphene.

CONCLUSION

In conclusion, STM imaging and spectroscopy revealed a new species of isolated FePc molecules on graphene on Ir. DFT calculations reproduce the experimental data and show that a nonclassic cycloaddition occurs between a C2 part of FePc and a C3 part of graphene. This new reaction is specific to the top-fcc area of the graphene layer. It is likely to occur with related molecules, e.g., metal porphyrins, as well.[35]

ASSOCIATED CONTENT

Supporting Information

Schemes of one- and two-lobe species, models and energetics of less stable cycloadducts. The Supporting Information is available free of charge on the ACS Publications website at DOI: 10.1021/jacs.5b05558.

AUTHOR INFORMATION

Corresponding Author

*berndt@physik.uni-kiel.de

Present Address

[§]Ecole Normale Supérieure-PSL Research University, Département de Chimie, Sorbonne Universités - UPMC Univ Paris 06, CNRS UMR 8640 PASTEUR, 24, rue Lhomond, 75005 Paris, France.

Notes

The authors declare no competing financial interest.

ACKNOWLEDGMENTS

We thank Noreen Singh and Shiri Burema for participating in the beginning of the project. S.J.A. and R.B. acknowledge financial support from the Deutsche Forschungsgemeinschaft via SFB 677. M.L.B. and M.L. are grateful for support from the ANR11-INTB-1014-01- Riderporh. Computer ressources have been provided by PSMN in ENS Lyon.

REFERENCES

(1) Geim, A. K. *Science* **2009**, *324*, 1530−1534.
(2) Englert, J. M.; Dotzer, C.; Yang, G.; Schmid, M.; Papp, C.; Gottfried, J. M.; Steinrück, H.-P.; Spiecker, E.; Hirsch, A.; Hauke, F. *Nat. Chem.* **2011**, *3*, 279−286.
(3) Niyogi, S.; Bekyarova, E.; Hong, J.; Khizroev, S.; Berger, C.; de Heer, W.; Haddon, R. C. *J. Phys. Chem. Lett.* **2011**, *2*, 2487−2498.
(4) Bekyarova, E.; Sarkar, S.; Niyogi, S.; Itkis, M. E.; Haddon, R. C. *J. Phys. D: Appl. Phys.* **2012**, *45*, 154009.
(5) Bekyarova, E.; Sarkar, S.; Wang, F.; Itkis, M. E.; Kalinina, I.; Tian, X.; Haddon, R. C. *Acc. Chem. Res.* **2013**, *46*, 65−76.
(6) Chua, C. K.; Pumera, M. *Chem. Soc. Rev.* **2013**, *42*, 3222−3233.
(7) Loh, K. P.; Bao, Q.; Ang, P. K.; Yang, J. *J. Mater. Chem.* **2010**, *20*, 2277−2289.
(8) Park, J.; Yan, M. *Acc. Chem. Res.* **2013**, *46*, 181−189.
(9) Swager, T. M. *ACS Macro Lett.* **2012**, *1*, 3−5.
(10) Gan, L.; Zhou, J.; Ke, F.; Gu, H.; Li, D.; Hu, Z.; Sun, Q.; Guo, X. *NPG Asia Mater.* **2012**, *4*, e31.
(11) Mao, H. Y.; Lu, Y. H.; Lin, J. D.; Zhong, S.; Wee, A. T. S.; Chen, W. *Prog. Surf. Sci.* **2013**, *88*, 132−159.
(12) Altenburg, S. J.; Berndt, R. *New J. Phys.* **2014**, *16*, 093047.
(13) Mao, J.; Zhang, H.; Jiang, Y.; Pan, Y.; Gao, M.; Xiao, W.; Gao, H.-J. *J. Am. Chem. Soc.* **2009**, *131*, 14136−14137.
(14) Karousis, N.; Ortiz, J.; Ohkubo, K.; Hasobe, T.; Fukuzumi, S.; Sastre-Santos, A.; Tagmatarchis, N. *J. Phys. Chem. C* **2012**, *116*, 20564−20573.
(15) Järvinen, P.; Hämäläinen, S. K.; Banerjee, K.; Häkkinen, P.; Ijäs, M.; Harju, A.; Liljeroth, P. *Nano Lett.* **2013**, *13*, 3199−3204.
(16) Li, B.; Tahara, K.; Adisoejoso, J.; Vanderlinden, W.; Mali, K. S.; De Gendt, S.; Tobe, Y.; De Feyter, S. *ACS Nano* **2013**, *7*, 10764−10772.
(17) Ogawa, Y.; Niu, T.; Wong, S. L.; Tsuji, M.; Wee, A. T. S.; Chen, W.; Ago, H. *J. Phys. Chem. C* **2013**, *117*, 21849−21855.
(18) Xiao, K.; Deng, W.; Keum, J. K.; Yoon, M.; Vlassiouk, I. V.; Clark, K. W.; Li, A.-P.; Kravchenko, I. I.; Gu, G.; Payzant, E. A.; Sumpter, B. G.; Smith, S. C.; Browning, J. F.; Geohegan, D. B. *J. Am. Chem. Soc.* **2013**, *135*, 3680−3687.
(19) Berger, C.; Song, Z.; Li, T.; Li, X.; Ogbazghi, A. Y.; Feng, R. *Science* **2006**, *312*, 1191.
(20) Nagashima, A.; Tejima, N.; Oshima, C. *Phys. Rev. B: Condens. Matter Mater. Phys.* **1994**, *50*, 17487.
(21) Marchini, S.; Günther, S.; Wintterlin, J. *Phys. Rev. B: Condens. Matter Mater. Phys.* **2007**, *76*, 075429.
(22) Preobrajenski, A. B.; Ng, M. L.; Vinogradov, A. S.; Mårtensson, N. *Phys. Rev. B: Condens. Matter Mater. Phys.* **2008**, *78*, 073401.
(23) Wintterlin, J.; Bocquet, M.-L. *Surf. Sci.* **2009**, *603*, 1841.
(24) Pletikosic, I.; Kralj, M.; Pervan, P.; Brako, R.; Coraux, J.; N'Diaye, A. T.; Busse, C.; Michely, T. *Phys. Rev. Lett.* **2009**, *102*, 056808.
(25) Altenburg, S. J.; Kröger, J.; Wang, B.; Bocquet, M.-L.; Lorente, N.; Berndt, R. *Phys. Rev. Lett.* **2010**, *105*, 236101.
(26) Altenburg, S. J.; Kröger, J.; Wehling, T. O.; Sachs, B.; Lichtenstein, A. I.; Berndt, R. *Phys. Rev. Lett.* **2012**, *108*, 206805.
(27) Woodward, R. B.; Hoffmann, R. *J. Am. Chem. Soc.* **1965**, *87*, 395−397.
(28) Woodward, R. B.; Hoffmann, R. *Science* **1970**, *167*, 825−831.
(29) Woodward, R. B.; Hoffmann, R. *J. Am. Chem. Soc.* **1965**, *87*, 2046−2048.
(30) Woodward, R. B.; Hoffmann, R. *J. Am. Chem. Soc.* **1965**, *87*, 4388−4389.
(31) Sarkar, S.; Bekyarova, E.; Niyogi, S.; Haddon, R. C. *J. Am. Chem. Soc.* **2011**, *133*, 3324−3327.
(32) Zhang, X.; Hou, L.; Cnossen, A.; Coleman, A. C.; Ivashenko, O.; Rudolf, P.; van Wees, B. J.; Browne, W. R.; Feringa, B. L. *Chem. - Eur. J.* **2011**, *17*, 8957−8964.
(33) Sarkar, S.; Bekyarova, E.; Haddon, R. C. *Acc. Chem. Res.* **2012**, *45*, 673−682.
(34) Scardamaglia, M.; Lisi, S.; Lizzit, S.; Baraldi, A.; Larciprete, R.; Mariani, C.; Betti, M. G. *J. Phys. Chem. C* **2013**, *117*, 3019−3027.
(35) Lattelais, M.; Bocquet, M.-L. *J. Phys. Chem. C* **2015**, *119*, 9234−9241.
(36) Busse, C.; Lazić, P.; Djemour, R.; Coraux, J.; Gerber, T.; Atodiresei, N.; Caciuc, V.; Brako, R.; N'Diaye, A. T.; Blügel, S.; Zegenhagen, J.; Michely, T. *Phys. Rev. Lett.* **2011**, *107*, 036101.
(37) Voloshina, E. N.; Fertitta, E.; Garhofer, A.; Mittendorfer, F.; Fonin, M.; Thissen, A.; Dedkov, Y. S. *Sci. Rep.* **2013**, *3*, 1072.
(38) Voloshina, E. N.; Dedkov, Y. S. *Phys. Chem. Chem. Phys.* **2012**, *14*, 13502−13514.
(39) Altenburg, S. J.; Berndt, R. *New J. Phys.* **2014**, *16*, 053036.
(40) Coraux, J.; N'Diaye, A. T.; Engler, M.; Busse, C.; Wall, D.; Buckanie, N.; zu Heringdorf, F.-J. M.; van Gastel, R.; Poelsema, B.; Michely, T. *New J. Phys.* **2009**, *11*, 023006.
(41) Kresse, G.; Furthmüller, J. *Comput. Mater. Sci.* **1996**, *6*, 15−50.
(42) Kresse, G.; Furthmüller, J. *Phys. Rev. B: Condens. Matter Mater. Phys.* **1996**, *54*, 11169.
(43) Kresse, G.; Joubert, D. *Phys. Rev. B: Condens. Matter Mater. Phys.* **1999**, *59*, 1758−1775.
(44) Perdew, J. P.; Burke, K.; Ernzerhof, M. *Phys. Rev. Lett.* **1996**, *77*, 3865−3868.
(45) Perdew, J. P.; Burke, K.; Ernzerhof, M. *Phys. Rev. Lett.* **1997**, *78*, 1396−1396.
(46) Grimme, S. *J. Comput. Chem.* **2006**, *27*, 1787−1799.

DOI: 10.1021/jacs.5b05558
J. Am. Chem. Soc. 2015, 137, 9452−9458

(47) Bucko, T. S.; Hafner, J. R.; Lebegut, S. B.; Angyan, J. N. G. *J. Phys. Chem. A* **2010**, *114*, 11814−11824.
(48) Stradi, D.; Díaz, C.; Martín, F.; Alcamí, M. *Theor. Chem. Acc.* **2011**, *128*, 497−503.
(49) Adamo, C.; Barone, V. *J. Chem. Phys.* **1999**, *110*, 6158−6170.
(50) Tsukahara, N.; Noto, K.; Ohara, M.; Shiraki, S.; Takagi, N.; Takata, Y.; Miyawaki, J.; Taguchi, M.; Chainani, A.; Shin, S.; Kawai, M. *Phys. Rev. Lett.* **2009**, *102*, 167203.
(51) Gopakumar, T.; Néel, N.; Kröger, J.; Berndt, R. *Chem. Phys. Lett.* **2009**, *484*, 59−63.
(52) Tsukahara, N.; Shiraki, S.; Itou, S.; Ohta, N.; Takagi, N.; Kawai, M. *Phys. Rev. Lett.* **2011**, *106*, 187201.
(53) Cheng, Z.; Du, S.; Guo, W.; Gao, L.; Deng, Z.; Jiang, N.; Guo, H.; Tang, H.; Gao, H. J. *Nano Res.* **2011**, *4*, 523−530.
(54) Gopakumar, T. G.; Brumme, T.; Kröger, J.; Toher, C.; Cuniberti, G.; Berndt, R. *J. Phys. Chem. C* **2011**, *115*, 12173−12179.
(55) Mugarza, A.; Robles, R.; Krull, C.; Korytár, R.; Lorente, N.; Gambardella, P. *Phys. Rev. B: Condens. Matter Mater. Phys.* **2012**, *85*, 155437.
(56) Isvoranu, C.; Ahlund, J.; Wang, B.; Ataman, E.; Måtensson, N.; Puglia, C.; Andersen, J. N. *J. Chem. Phys.* **2009**, *131*, 214709−214707.
(57) Tekiel, A.; Goryl, M.; Szymonski, M. *Nanotechnology* **2007**, *18*, 475707.
(58) Gruyters, M.; Pingel, T.; Gopakumar, T. G.; Néel, N.; Schütt, C.; Köhler, F.; Herges, R.; Berndt, R. J. *J. Phys. Chem. C* **2012**, *116*, 20882−20886.
(59) N'Diaye, A. T.; Coraux, J.; Plasa, T. N.; Busse, C.; Michely, T. *New J. Phys.* **2008**, *10*, 043033.
(60) Zhao, A.; Li, Q.; Chen, L.; Xiang, H.; Wang, W.; Pan, S.; Wang, B.; Xiao, X.; Yang, J.; Hou, J. G.; Zhu, Q. *Science* **2005**, *309*, 1542−1544.
(61) Wang, Y. F.; Kröger, J.; Berndt, R.; Vázquez, H.; Brandbyge, M.; Paulsson, M. *Phys. Rev. Lett.* **2010**, *104*, 176802.
(62) Sperl, A.; Kröger, J.; Berndt, R. *Angew. Chem., Int. Ed.* **2011**, *50*, 5294−5297.
(63) Feibelman, P. J. *Phys. Rev. B: Condens. Matter Mater. Phys.* **2008**, *77*, 165419.

DOI: 10.1021/jacs.5b05558
J. Am. Chem. Soc. 2015, 137, 9452−9458